

# Proton image and momentum distributions from light-front dynamics

E. Ydrefors<sup>1,\*</sup> and T. Frederico<sup>1,†</sup>

<sup>1</sup>*Instituto Tecnológico de Aeronáutica, DCTA, 12228-900 São José dos Campos, Brazil*

(Dated: March 29, 2022)

We apply a dynamical three-constituent quark light-front model to study the proton. The dynamics is based on the notion of a diquark as the dominant interaction channel to build the three-body Faddeev Bethe-Salpeter equations for the valence state, and we focus on the totally symmetric part of the wave function. The Dirac electromagnetic form factor is used to fix the model parameters, and the valence wave function is obtained. From that we investigate its Ioffe-time image, non-polarized longitudinal and transverse momentum distributions, and the double momentum distribution.

Keywords: Bethe-Salpeter equation, pion valence state, proton structure, Ioffe-time distribution, momentum distribution

## I. INTRODUCTION

The complex nucleon wave function on the null-plane ( $x^+ = t + z = 0$ ) expressed in the Fock space in terms of its constituent degrees of freedom, namely quarks and gluons at a given scale  $\mu$  and strongly interacting, ultimately provides the image through the associated probability densities [1–3]. The relevant degrees of freedom at the hadronic scale are the dressed constituents, which carry the complex infrared (IR) physics, confinement and spontaneous chiral symmetry breaking reflected in the large dressing of the light-flavored quarks and in the nucleon mass [3]. It is also well known the large IR dressing of the gluon as computed with lattice QCD (for a recent discussion of the gluon propagator in the Landau gauge see [4]).

The light-front (LF) wave function is an eigenstate of the mass squared operator and the compatible operators  $\vec{P}$  (momentum),  $J^2$  (squared angular momentum),  $J_z$  and other compatible operators like the parity. However,  $P_z$ ,  $\vec{J}_\perp$  and parity are not diagonal in the Fock space, i.e. they contain the interaction [1, 2]. Although simple to state, still today the connection between QCD in Euclidean space, their infrared (IR) properties, with the LF wave function, and its Fock decomposition is yet a challenge for our understanding, beyond the large momentum behavior that thanks to the asymptotic freedom is well known, like the counting rules (see e.g. [1]) as well as the ultraviolet (UV) behavior of the Fock amplitudes [5].

Ideally the LF nucleon wave function onto the null-

plane should have an infinite number of Fock-state components that evolves with the scale  $\mu$ . The wave function can be decomposed into Fock components each one associated with a probability amplitude  $\Psi_n(x_1, \vec{k}_{1\perp}, x_2, \vec{k}_{2\perp}, \dots; \mu)$  for  $n \geq 3$  partons, which is invariant under LF kinematical boosts. The probability corresponding to each Fock component is given by:

$$P_n(\mu) = \left\{ \prod_{i=1}^n \int \frac{d^2 k_i}{(2\pi)^2} \int_0^1 dx_i \right\} \delta \left( 1 - \sum_{i=1}^n x_i \right) \times \delta \left( \sum_{i=1}^n \vec{k}_{i\perp} \right) |\Psi_n(x_1, \vec{k}_{1\perp}, x_2, \vec{k}_{2\perp}, \dots; \mu)|^2, \quad (1)$$

where the transverse momentum of the constituent is  $\vec{k}_{i\perp}$  and its momentum fraction  $x_i$ . The valence component corresponds to  $n = 3$ . For simplicity, we have not depicted the dependence on the polarization state of the nucleon, as well as its constituents. The probability for each Fock component is  $P_n(\mu)$ , where we kept the scale dependence. At the hadron scale ( $\sim \Lambda_{QCD}$ ) the dominant component is the valence one, and for example in the pion case it amounts to about 70% as it has been computed recently in a Bethe-Salpeter framework [6]. The total normalization is  $\sum_{i \geq 3}^\infty P_n(\mu) = 1$ .

Each Fock amplitude can be written in the configuration space associated with the null-plane, where the three-dimensional position coordinates for each constituent are  $\{b_i^-, \vec{b}_{i\perp}\}$ , namely the light-like coordinate ( $b_i^- = t - z$ ) and transverse position ( $\vec{b}_{i\perp}$ ), conjugate to  $k_i^+ = x_i p^+$  and  $\vec{k}_{i\perp}$ , respectively.

\* ydrefors@kth.se

† tobias@ita.br

The Fock component of the wave function on the null-plane is obtained by a Fourier transform:

$$\begin{aligned} \tilde{\Psi}_n(\tilde{x}_1, \vec{b}_{1\perp}, \dots; \mu) = & \\ \left\{ \prod_{i=1}^n \int \frac{d^2 k_i}{(2\pi)^2} \int_0^1 \frac{dx_i}{2\pi} e^{i\tilde{x}_i x_i - i\vec{b}_{i\perp} \cdot \vec{k}_{i\perp}} \right\} & \quad (2) \\ \times \delta\left(1 - \sum_{i=1}^n x_i\right) \delta\left(\sum_{i=1}^n \vec{k}_{i\perp}\right) \Psi_n(x_1, \vec{k}_{1\perp}, \dots; \mu), \end{aligned}$$

where the dependence on the Ioffe time  $\tilde{x}_i = b_i^- p^+$  [7–9] was given in the probability amplitude instead of the light-like position onto the null-plane. The probability densities  $|\tilde{\Psi}_n(\tilde{x}_1, \vec{b}_{1\perp}, \dots; \mu)|^2$  build an image of the nucleon on the null-plane, where the light-like coordinate, shows the relevance of the Ioffe time to complete the image of the nucleon (see a recent general discussion in [10] and in the case of the pion in [6]). The Ioffe time was recently applied to obtain the pion valence PDF from lattice QCD (LQCD) in [11].

Different parton probability densities, namely one-, two- and N-body ones can be defined given the LF wave function and reveal the multifaceted structure of the nucleon, which are associated with different observables being of interest not only for the present hadron facilities but also for the physics cases of the future Electron Ion Collider [12]. In particular, we mention the electromagnetic ones, as for example the elastic form factor, and the parton distributions which are associated with one-body probability densities.

Other quantities related to the LF wave function appear in the deeply virtual Compton scattering (DVCS) or semi-inclusive deeply inelastic scattering (SIDIS), associated with the generalized parton distributions (GPDs) [13], the generalized transverse momentum distributions GTMDs [14–17], and this last one includes the elastic form factor, PDFs and GPDs.

In particular, we remind that the space-like electromagnetic form factor can be obtained from the celebrated Drell-Yan-West formula [1] using the "plus" component of the current, with momentum  $q^+ = 0$  and  $q^2 = -\vec{q}_\perp^2 = -Q^2$ , which is diagonal in the Fock space:

$$\begin{aligned} F(Q^2) = \sum_{n=3}^{\infty} F_{(n)}(Q^2) = \sum_{n=3}^{\infty} \sum_{j=1}^n e_j & \\ \times \left\{ \prod_{i=1}^n \int \frac{d^2 k_i}{(2\pi)^2} \int_0^1 dx_i \right\} \delta\left(1 - \sum_{i=1}^n x_i\right) & \quad (3) \\ \times \delta\left(\sum_{i=1}^n \vec{k}_{i\perp}^f\right) \Psi_n^\dagger(x_1, \vec{k}_{1\perp}^f, x_2, \vec{k}_{2\perp}^f, \dots, x_j, \vec{k}_{j\perp}^f, \dots) & \\ \times \Psi_n(x_1, \vec{k}_{1\perp}^i, x_2, \vec{k}_{2\perp}^i, \dots, x_j, \vec{k}_{j\perp}^i, \dots), \end{aligned}$$

where the number of constituents in the Fock components are  $n \geq 3$ , and  $e_j$  is the constituent charge in units of the fundamental charge. The partial contribution to the form factor from each Fock component of the wave function is  $F_{(n)}(Q^2)$ . The quark momenta obtained via the LF boost from the Breit-frame to the rest-frame of the initial (i) and final (f) nucleon states are given by:

$$\begin{aligned} \vec{k}_{i\perp}^i &= \vec{k}_{i\perp} + \frac{\vec{q}_\perp}{2} x_i, \quad \vec{k}_{i\perp}^f = \vec{k}_{i\perp} - \frac{\vec{q}_\perp}{2} x_i; \quad i \neq j \\ \text{and } \vec{k}_{j\perp}^f &= (-) \frac{\vec{q}_\perp}{2} (1 - x_j) - \sum_{i \neq j} \vec{k}_{i\perp}, \end{aligned} \quad (4)$$

with the transverse momentum of the quark that absorbed the virtual photon being:  $\vec{k}_{j\perp} = \pm \frac{\vec{q}_\perp}{2} - \sum_{i \neq j} \vec{k}_{i\perp}$ , with + and – meaning the momentum in the initial and final hadron states, respectively. For each Fock component of the LF wave function the transverse momenta add up to  $\sum_{j=1}^n \vec{k}_{j\perp}^i = \sum_{j=1}^n \vec{k}_{j\perp}^f = \vec{0}_\perp$ , for the rest-frames of the initial and final hadron states. The normalized wave function gives  $F(0) = 1$ .

Beyond the electromagnetic processes, proton-proton collisions performed at the Large Hadron Collider in its high-luminosity phase requires a detailed consideration of the nucleon structure for the understanding of the observed data, associated with multiple parton interactions (MPIs), which are required for the description of hadronic final states (see e.g. [18]).

MPIs become more important for high-energy collisions as the parton flux increases, while the parton momentum fractions decrease, as the nucleon momentum is shared among more participants. Therefore, the search for new physics demands the consideration of MPIs in the dedicated experimental analysis (see the review book on Multiple Parton Interactions at the LHC [19]). One example, is the double parton scattering (DPS) in hadron-hadron collisions, where two independent hard-scattering processes happen between partons from a parton pair in each hadron. It receives contributions from all LF Fock-components of each hadron wave function, and such information is encoded in the double parton distribution function [20].

The DPS cross section depends on the double parton distribution functions (dPDFs) contain contributions from all Fock-component of the wave function,

and it is written as [20]:

$$\begin{aligned}
D(x_1, x_2, \vec{q}_\perp) &= \sum_{n=3}^{\infty} D_n(x_1, x_2, \vec{q}_\perp) = \\
&\sum_{n=3}^{\infty} \int \frac{d^2 k_1}{(2\pi)^2} \frac{d^2 k_2}{(2\pi)^2} \left\{ \prod_{i \neq 1,2} \int \frac{d^2 k_i}{(2\pi)^2} \int_0^1 dx_i \right\} \\
&\times \delta \left( 1 - \sum_{i=1}^n x_i \right) \delta \left( \sum_{i=1}^n \vec{k}_{i\perp} \right) \\
&\times \Psi_n^\dagger(x_1, \vec{k}_{1\perp} + \vec{q}_\perp, x_2, \vec{k}_{2\perp} - \vec{q}_\perp, \dots) \\
&\times \Psi_n(x_1, \vec{k}_{1\perp}, x_2, \vec{k}_{2\perp}, \dots),
\end{aligned} \tag{5}$$

where for simplicity we have not depicted the polarization states for neither the constituents nor the hadron itself. The Fourier transform of  $D(x_1, x_2, \vec{q}_\perp)$  in  $\vec{q}_\perp$  gives the probability of finding the constituents 1 and 2 with momentum fraction  $x_1$  and  $x_2$  at a relative distance in the transverse direction  $\vec{y}_\perp$  within the hadron state. The quantity  $D_n(x_1, x_2, \vec{q}_\perp)$  is contribution from a given Fock-component of the LF wave function to the double parton distribution.

In terms of operator product the double distribution reads [21]:

$$\begin{aligned}
\tilde{D}(x_1, x_2, \vec{y}_\perp) &= 2p^+ \int dy^- \int \frac{dz_1^-}{2\pi} \frac{dz_2^-}{2\pi} \\
&\times e^{i(x_1 z_1^- + x_2 z_2^-)p^+} \sum_{\lambda} \langle p, \lambda | \mathcal{O}(y, z_1) \mathcal{O}(0, z_2) | p, \lambda \rangle,
\end{aligned} \tag{6}$$

which has been obtained for the nucleon by recent LQCD calculations for different operator structures [21]. Despite such efforts, it is useful to obtain the dPDFs at the nucleon scale and identifying properties of the LF wave function, as for example using AdS/QCD approach [22] and LF constituent quark models (see e.g. [23]). Among such efforts to detail the LF wave function within a dynamical framework, we should mention the Basis Light-Front Quantization applied to QCD [24] and recently used to study the nucleon [25].

Motivated by the above discussion, our goal in this work is to explore the consequences of the relativistic LF three-body dynamics in the structure of the valence state of the nucleon, by studying one- and two-quark momentum distributions, where effectively the interaction is dominated by a strong scalar quark-quark correlation. This model relies on the use of the contact interaction between the constituents within the Faddeev Bethe-Salpeter approach

on the light-front [26–29], and more recently the model was extended beyond the valence state in Euclidean space [30] and in Minkowski space [31, 32]. For practical applications, the profile of the IR momentum dependence of the valence wave function, as for instance computed from the transverse amplitude, obtained by both the LF truncation and the full four-dimensional approach are essentially equivalent, once the bound state binding energy are close [30], which will be enough for the present study. As a note, we observe that short-range correlations between two quarks are present in the model, in analogy with the nucleon-nucleon short-range correlations (see e.g. [33]), which have also its counterpart in the relativistic three-body wave function [32], with the proviso that the UV behavior has to be viewed with caution as the scaling laws [5] from QCD are not built-in.

The adopted effective LF model emphasizes the IR dynamics of constituent quarks with a dominant scalar diquark correlation. Indeed, one main feature that the continuum approaches to QCD have been teaching us is that two-quark correlations, namely, diquarks, which are not asymptotic states, are known to play a relevant role in the structure and dynamics of the nucleon (see e.g. [34] and the recent review [35]).

We should remind that the successful Nambu-Jona-Lasinio model applied to investigate phenomenological aspects of QCD in the IR region [36], embodies the dynamical chiral symmetry breaking by producing massive constituent ( $m \sim 300$  MeV) for the  $u$  and  $d$  quarks and pions/kaons as Goldstone bosons, bringing in addition diquarks, with the favored one being the scalar color antitriplet ( $[ud]_{0+}^{\bar{3}_c}$ ) state. We see the renewed interest from LQCD groups in determining the properties of diquarks in a gauge invariant way [37] gives at the physical pion mass a difference of 319(1) MeV between the mass of the lightest diquark,  $[ud]_{0+}^{\bar{3}_c}$ , and the light antiquark, and a size of about one fm. The low-energy diquark effective degree of freedom has also been invoked to smooth the transition between the hadron to quark phases of dense matter (see Ref. [38]).

The model adopted in this work considers the formation of a bound diquark or a virtual state as the main dynamical characteristic, which is in line with modern evidences of the relevance of the  $[ud]_{0+}^{\bar{3}_c}$  state in the IR properties of the quark-quark effective interaction within the nucleon. We aim to explore the proton bound-state structure in terms of constituent quarks degrees of freedom by calculating the valence LF wave function, where our focus is to study its Ioffe

time representation, as well as the different one- and two-quark momentum distributions.

The rest of this work is organized as follows. A brief presentation of the LF three-quark model is given in section II, containing the description of the homogeneous LF Faddeev integral equation and numerical results for the vertex Faddeev component. The results for the distribution amplitude and Ioffe-time image of the proton are given in section III. The calculations of the valence Dirac form factor of the proton are discussed in IV. The results for the momentum distributions, namely valence parton distribution, valence double parton distribution and transverse momentum distributions for single and two quarks are shown in section V. The main points of our work are summarized in section VI.

## II. BRIEF PRESENTATION OF THE LF THREE-QUARK MODEL

The model adopted to investigate the Ioffe time representation of the wave function and also the double parton distribution, is based on the contact interaction between the constituent quarks, where the spin degree of freedom is not taken into account, as it is our aim to study the spatial non-polarized distribution of the quarks in the valence state. In the model we consider only the totally symmetric momentum part of the colorless three-quark wave function corresponding to the valence nucleon state, as we are interested for the time being on the investigation of the properties associated with the momentum distributions and the image of the nucleon onto the null-plane. The model wave function is given by [32]:

$$\Psi_3(x_1, \vec{k}_{1\perp}, x_2, \vec{k}_{2\perp}, x_3, \vec{k}_{3\perp}) = \frac{\Gamma(x_1, \vec{k}_{1\perp}) + \Gamma(x_2, \vec{k}_{2\perp}) + \Gamma(x_3, \vec{k}_{3\perp})}{\sqrt{x_1 x_2 x_3} (M_N^2 - M_0^2(x_1, \vec{k}_{1\perp}, x_2, \vec{k}_{2\perp}, x_3, \vec{k}_{3\perp}))}, \quad (7)$$

where  $\Gamma(x_i, \vec{k}_{i\perp})$  is the Faddeev component of the vertex function for the bound state,  $x_1 + x_2 + x_3 = 1$ ,  $\vec{k}_{1\perp} + \vec{k}_{2\perp} + \vec{k}_{3\perp} = \vec{0}_\perp$  and

$$M_0^2(x_1, \vec{k}_{1\perp}, x_2, \vec{k}_{2\perp}, x_3, \vec{k}_{3\perp}) = \frac{\vec{k}_{1\perp}^2 + m^2}{x_1} + \frac{\vec{k}_{2\perp}^2 + m^2}{x_2} + \frac{\vec{k}_{3\perp}^2 + m^2}{x_3}, \quad (8)$$

is the free three-body squared mass for on-mass-shell constituents. The factorized form of the valence wave function, namely with a vertex function depending

solely on the bachelor quark LF momenta, is a consequence of the effective contact interaction between the constituent quarks, which is an idealized model resembling the successful Nambu-Jona-Lasinio model applied to model QCD [36]. It should be understood as an effective low-energy model which is meant to have significance in the IR region where constituent quarks are massive and bound forming the nucleon.

### A. Homogeneous LF Faddeev integral equation

The Faddeev equation for the vertex component of the valence LF wave function is given by [26, 29]:

$$\Gamma(k_\perp, x) = \frac{\mathcal{F}(M_{12}^2)}{(2\pi)^3} \int_0^{1-x} \frac{dx'}{x'(1-x-x')} \times \int_0^\infty d^2 k'_\perp \frac{\Gamma(k'_\perp, x)}{\widehat{M}_0^2 - M_N^2}, \quad (9)$$

where

$$\widehat{M}_0^2 = M_0^2(x, \vec{k}_\perp, x', \vec{k}'_\perp, 1-x-x', -(\vec{k}_\perp + \vec{k}'_\perp)), \quad (10)$$

and the two-quark amplitude has the expression

$$\mathcal{F}(M_{12}^2) = \frac{\Theta(-M_{12}^2)}{\frac{1}{16\pi^2 y} \log \frac{1+y}{1-y} - \frac{1}{16\pi m a}} + \frac{\Theta(M_{12}^2) \Theta(4m^2 - M_{12}^2)}{\frac{1}{8\pi^2 y'} \arctan y' - \frac{1}{16\pi m a}}, \quad (11)$$

with its argument, the effective off-shell mass of the two-quark subsystem squared, given by

$$M_{12}^2 = (1-x)M_N^2 - \frac{k_\perp^2 + (1-x)m^2}{x}, \quad (12)$$

$$y = \frac{M_{12}}{\sqrt{4m^2 - M_{12}^2}} \quad \text{and} \quad y' = \frac{\sqrt{-M_{12}^2}}{\sqrt{4m^2 - M_{12}^2}}.$$

The kernel of the LF Faddeev equation (9) contains the quark exchange mechanism expressed by the presence of the three-quark LF resolvent, namely the operator  $[\widehat{M}_0^2 - M_N^2]^{-1}$ . Consistently with the adopted model, it is well known [34] that the four-dimensional formulation the three-quark Bethe-Salpeter equation presents the quark exchange kernel, when the diquarks dominates the quark-quark interaction.

The quark-quark scattering amplitude,  $\mathcal{F}(M_{12}^2)$ , weights the Faddeev LF integral equation and carries the pole of the bound or virtual diquark, that depends

Model	$m$ [MeV]	$a$ [ $m^{-1}$ ]	$M_2$ [MeV]	$M_N$ [m]	$r_{F_1}$ [fm]
I	317	-1.84	-	2.97	0.97
II	362	3.60	681	2.60	0.72

TABLE I. Constituent mass in MeV, scattering length, diquark mass, and three-body mass for the two considered models. Our diquark mass for model II is slightly smaller than the scalar diquark mass of 691 MeV obtained in [39]. Also shown is the radius defined as  $r_{F_1} = \hbar c \sqrt{-6 \frac{dF_1}{dQ^2}}|_{Q^2=0}$  and the corresponding experimental value is 0.757 fm [40].

on the scattering length  $a$ , which can be either positive or negative. If  $a > 0$ , the quark-quark system is bound and the nucleon will be described as a quark-diquark system. On the contrary if  $a$  is negative no physical two-body bound-state exists and the nucleon is thus a Borromean state. In both cases,  $\mathcal{F}(M_{12}^2)$  has a pole, for  $a > 0$  in the physical complex-energy sheet and for  $a < 0$  in the 2<sup>nd</sup> sheet, meaning the virtual state. Therefore, in either case the strong diquark correlation is present in the model and should be interpreted as dominating the IR properties of the nucleon. Both of these two cases will be investigated in this paper. An earlier study of the nucleon performed with a truncated form of Eq. (9) was performed in [27].

### B. Vertex Faddeev component

The structure of the three-quark valence state is encoded in the vertex function  $\Gamma(k_\perp, x)$ , which was computed with the two parameter sets from Table I. The constituent quark masses are 317 MeV (model I) and 362 MeV (model II) to be compared with about 350 MeV from a recent LQCD calculation in the Landau gauge [41]. We choose two possibilities for diquarks, namely an unbound one for  $a < 0$  and a bound one for  $a > 0$ , with a diquark mass of 681 MeV. These parameters are found by reproducing qualitatively the space-like Dirac form factor up to about 1 GeV<sup>2</sup>, as it will be shown later on. We observe that, the diquark mass of 681 MeV, which has a difference of 319 MeV with respect to the quark mass, coincidentally matches the gauge invariant result from the LQCD calculation [37] of 319(1) MeV at the physical pion mass.

The results for the vertex function  $\Gamma(k_\perp, x)$  are shown in Fig. 1 for models I (lower panel) and II (upper panel). The vertex function for both mod-

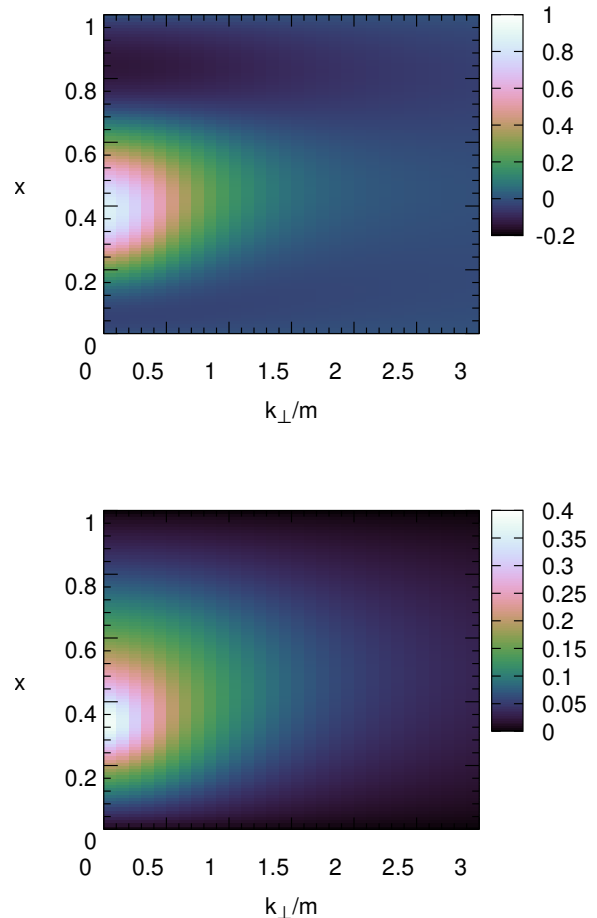


FIG. 1. Vertex function,  $\Gamma(k_\perp, x)$ , for the model I (lower panel) and II (upper panel).

els has characteristic transverse momentum around the IR scale of  $\sim \Lambda_{QCD}$ , which drives the decreasing behaviour with  $k_\perp$ . In addition, the vertex function peaks between  $x \sim 0.35 - 0.4$ , and the peak evolves to somewhat larger values of  $x$  with  $k_\perp$ , as a consequence of the dominance of  $k_\perp^2/x$  in the free squared mass operator, which comes with the quark exchange kernel, as should be a general feature of the diquark (bound or virtual) dominance in the quark-quark interaction.

It is seen in the right panel of Fig. 1 that for model II with  $a > 0$ , there is one node around  $x = 0.8$  and also one for small  $x$ . As studied in detail in Ref. [30], for  $a > 0$  the physical ground state of (9) is not the lowest energy solution of the equation. That is, it exists an-

other unphysical solution with  $M_N^2 < 0$ . This state is the relativistic analog of the well-known Thomas collapse in non-relativistic three-body systems with zero-range interaction [42]. For example, at  $1/(am) = 0.26$  one has  $M_N^2 = -69 m^2$ , so it is a very deep state. In principle, it should be possible to remove this state by a momentum cut-off  $\Lambda$  of the order of 1 GeV, which would weaken the interaction in the short-range region.

### III. DISTRIBUTION AMPLITUDE AND IOFFE-TIME IMAGE

#### A. Distribution amplitude

The distribution amplitude (DA),  $\phi(x_1, x_2)$  for the nucleon is defined as

$$\phi(x_1, x_2) = \int d^2 k_{1\perp} d^2 k_{2\perp} \Psi_3(x_1, \vec{k}_{1\perp}, x_2, \vec{k}_{2\perp}, x_3, \vec{k}_{3\perp}) \quad (13)$$

and obeys the symmetry relation

$$\phi(x_1, x_2) = \phi(x_2, x_1). \quad (14)$$

It gives the dependence of the wave function on the longitudinal momentum fraction when the quarks share the same transverse position. In Fig. 2, the calculated DA is shown for the two models considered in the present work. In the figure the DA was normalized so that  $\int_0^1 dx_1 \int_0^{1-x_1} dx_2 \phi(x_1, x_2) = 1$ . The two different models give similar results with a slightly wider distribution for model II, which reflects the wave function behaviour close to  $x_i \sim 0$ . Further insight comes with the Fourier transform as discussed in what follows.

#### B. Ioffe-time image of the valence state

For the study of the space-time structure of the proton it is of interest to obtain the wave function in terms of the Ioffe-times ( $\tilde{x}_1$  and  $\tilde{x}_2$ ) and the transverse coordinates ( $\vec{b}_{1\perp}$  and  $\vec{b}_{2\perp}$ ). Such study has been performed recently for the pion [6]. This is accomplished through the Fourier transform of  $\Psi_3(x_1, \vec{k}_{1\perp}; x_2, \vec{k}_{2\perp}; x_3, \vec{k}_{3\perp})$ . For simplicity, we consider here the particular case:

$$\Phi(\tilde{x}_1, \tilde{x}_2) \equiv \tilde{\Psi}_3(\tilde{x}_1, \vec{0}_\perp, \tilde{x}_2, \vec{0}_\perp) = \int_0^1 dx_1 e^{i\tilde{x}_1 x_1} \int_0^{1-x_1} dx_2 e^{i\tilde{x}_2 x_2} \phi(x_1, x_2), \quad (15)$$

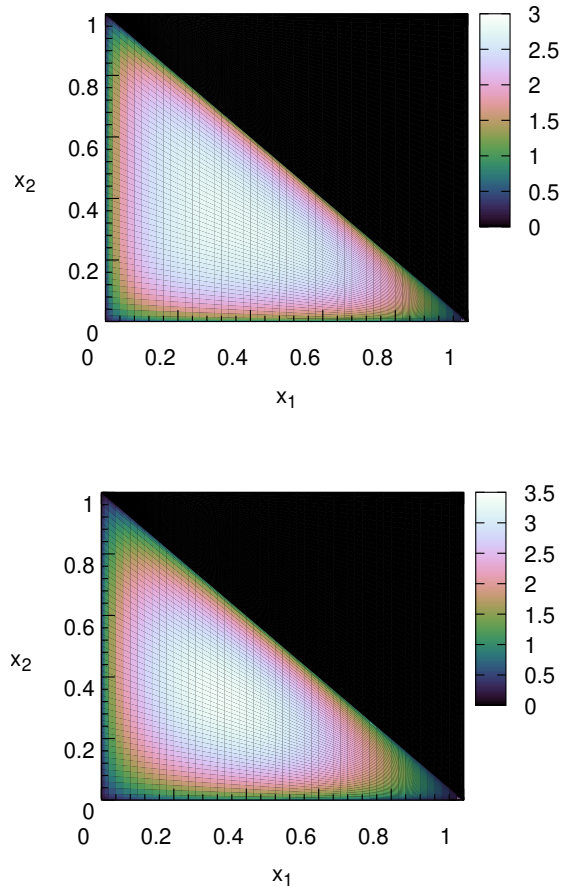


FIG. 2. Distribution amplitude as a function of  $x_1$  and  $x_2$ , for the model I (lower panel) and for model II (upper panel).

where the configuration space wave function is computed at the origin  $\vec{b}_{1\perp} = \vec{b}_{2\perp} = \vec{0}_\perp$ .

In Fig. 3 we present our results for the squared modulus of the Ioffe-time distribution given by Eq. (15). In the upper panel is shown the 3D plot of the distribution in terms of the variables  $\tilde{x}_1$  and  $\tilde{x}_2$  for model I. It is clear the preference of quarks to minimize the relative distance in Ioffe time, as also observed along  $\tilde{x}_1 = \tilde{x}_2$ . The decrease along the just reflects the presence of the third quark that recoils as the center of mass is at rest. Notably, there is no perceptible difference in this plot between model I and II.

Then, in the lower panel of Fig. 3 we show for both models the Ioffe-time distribution as a function of  $\tilde{x}_1$  for two fixed values of  $\tilde{x}_2$ , namely  $\tilde{x}_2 = 0$  and  $\tilde{x}_2 = 10$ . It is seen that the results obtained with the two parameter sets are almost identical for

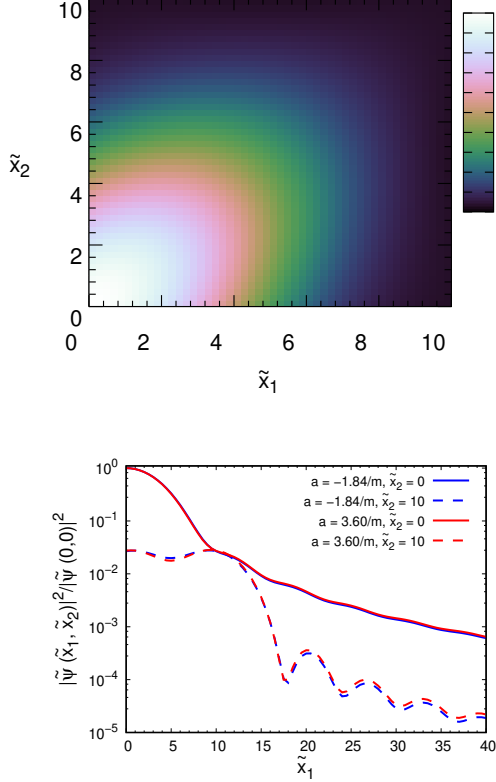


FIG. 3. Upper panel: Squared modulus of the Ioffe-time distribution as a function of  $\tilde{x}_1$  and  $\tilde{x}_2$ , for the model I. Lower panel: Squared modulus of the Ioffe-time distribution as a function of  $\tilde{x}_1$  for two fixed values of  $\tilde{x}_2$ , namely  $\tilde{x}_2 = 0$  (solid line) and  $\tilde{x}_2 = 10$  (dashed line). Results shown for the model I (blue line) and model II (red line).

$\tilde{x}_1 < 17$ . In addition, we observe the equality between the  $|\tilde{\phi}(0, 10)| = |\tilde{\phi}(10, 0)| = |\tilde{\phi}(10, 10)|$ , which comes from the permutation symmetry of the wave function:

$$|\tilde{\phi}(\tilde{x}, 0)| = |\tilde{\phi}(0, \tilde{x})| = |\tilde{\phi}(\tilde{x}, \tilde{x})|, \quad (16)$$

which is a general characteristic of the model. This explains also the rough flat behavior of  $|\tilde{\phi}(\tilde{x}_1, 10)|$  for  $0 < \tilde{x}_1 < 10$  (dashed line).

For  $\tilde{x}_2 = 10$  (dashed lines in Fig. 3) a sizable decrease of the magnitude is observed at  $\tilde{x}_1 > 10$  and for larger values an oscillatory behavior is seen. This reflects the size of the nucleon of about 1 fm and a mass of 1 GeV, with their dimensionless product taking into account the factor 1/2 from the adopted metric  $\lambda^{-1} \sim 0.1$  with the characteristic oscillatory pattern having a wave length in Ioffe time of about 10,

which is observed in the figure. This is also roughly the dimensionless scale, which governs the decrease of the wave function in the two quarks relative separation in Ioffe time.

Both trends, namely oscillation and damping of the wave function are essentially the same for models I and II, as their proton charge radius are somewhat close, besides the same nucleon mass, as seen in Table I. It suggests that this general behavior should be quite model independent. Notably, a similar qualitative behavior of the Ioffe-time distribution for the pion was obtained in [6]. We observe an exponential damping of the probability density with the relative separation between the Ioffe time of the two quarks, and the damping is expected to be more sizable if confinement is incorporated as it is effective at large distances.

#### IV. VALENCE DIRAC FORM FACTOR OF THE PROTON

In the three-body null-plane model, i.e. only taking into account the valence contribution ( $n = 3$ ) in the form factor formula (3), the Dirac form factor is given by:

$$F_1(Q^2) = \left\{ \prod_{i=1}^3 \int \frac{d^2 k_i}{(2\pi)^2} \int_0^1 dx_i \right\} \delta \left( 1 - \sum_{i=1}^3 x_i \right) \times \delta \left( \sum_{i=1}^3 \vec{k}_{i\perp}^f \right) \Psi_3^\dagger(x_1, \vec{k}_{1\perp}^f, \dots) \Psi_3(x_1, \vec{k}_{1\perp}^i, \dots), \quad (17)$$

with  $Q^2 = \vec{q}_\perp \cdot \vec{q}_\perp$ . In Eq. (4) the transverse momentum of the quarks in the Breit frame are given.

One has in Eq. (17) that  $d^2 k_{i\perp} = |\vec{k}_{i\perp}| d|\vec{k}_{i\perp}| d\theta_i$  ( $i = 1, 2$ ) with  $\vec{k}_{i\perp} \cdot \vec{q}_\perp = |\vec{k}_{i\perp}| |\vec{q}_\perp| \cos \theta_i$ . Additionally, the needed magnitudes of the transverse momenta are given by

$$\begin{aligned} |\vec{k}_{i\perp}^{f(i)}|^2 &= \left| \vec{k}_{i\perp} \pm \frac{\vec{q}_\perp}{2} x_i \right|^2 \\ &= \vec{k}_{i\perp}^2 + \frac{Q^2}{4} x_i^2 \pm x_i |\vec{k}_{i\perp}| |\vec{q}_\perp| \cos \theta_i, \end{aligned} \quad (18)$$

with  $-$  for f and  $+$  for i, in addition we have

$$\begin{aligned} |\vec{k}_{3\perp}^{f(i)}|^2 &= \left| \pm \frac{\vec{q}_\perp}{2} (x_3 - 1) - \vec{k}_{1\perp} - \vec{k}_{2\perp} \right|^2 = \\ &= (1 - x_3)^2 \frac{Q^2}{4} + \vec{k}_{1\perp}^2 + 2|\vec{k}_{1\perp}| |\vec{k}_{2\perp}| \cos(\theta_1 - \theta_2) \\ &+ \vec{k}_{2\perp}^2 \pm (1 - x_3) |\vec{q}_\perp| (|\vec{k}_{1\perp}| \cos \theta_1 + |\vec{k}_{2\perp}| \cos \theta_2). \end{aligned} \quad (19)$$

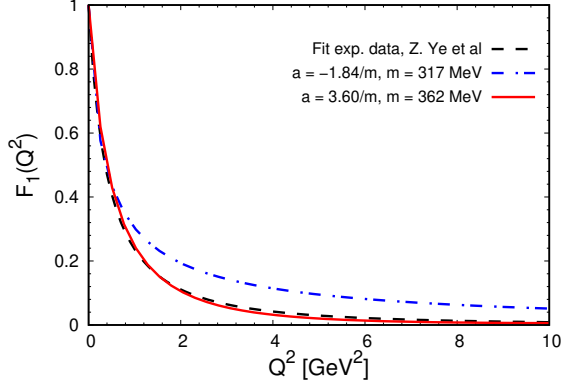


FIG. 4. Computed  $F_1(Q^2)$  (solid and dot-dashed lines) compared with the empirical fit (dashed line) obtained in Ref. [43].

In Fig. 4, the computed Dirac form factor,  $F_1(Q^2)$ , for the two parameter sets listed in Table I, is compared with the global fit to experimental data by Ye et al [43]. It is seen that model I with  $a = 3.60/m$  gives a quite good agreement with the experimental data. This thus favors the description of the nucleon as a quark-diquark system. The computed values of the radius  $r_{F_1} = \hbar c \sqrt{-6 \frac{dF_1}{dQ^2} |_{Q^2=0}}$  for the two considered models are also listed in Table I. The model II gives a radius of 0.72 fm which is about 5% lower than the experimental value of 0.757 fm [40] from the charge form factor. On the contrary, for the first model with  $a < 0$  a rather large radius of 0.97 fm was obtained. We could have attempted to fit the charge radius from  $F_1$ , by changing the constituent quark mass and scattering length. However, we choose to keep the qualitative reproduction of the form factor up to  $Q^2 \sim 1 \text{ GeV}^2$ , which should be the scale of our model.

## V. MOMENTUM DISTRIBUTIONS

### A. Valence parton distribution

We study next the decomposition of the single parton distribution function (PDF), obtained from the integrand of Eq. (17) of the Dirac form factor:

$$f_1(x_1) = \frac{1}{(2\pi)^6} \int_0^{1-x_1} dx_2 \int d^2 k_{1\perp} d^2 k_{2\perp} \times |\Psi_3(x_1, \vec{k}_{1\perp}, x_2, \vec{k}_{2\perp}, x_3, \vec{k}_{3\perp})|^2 \quad (20)$$

$$= I_{11} + I_{22} + I_{33} + I_{12} + I_{13} + I_{23}.$$

where the contributions to the PDF are defined for  $i = 1, 2, 3$  as:

$$I_{ii} = \frac{1}{(2\pi)^6} \int_0^{1-x_1} \frac{dx_2}{x_1 x_2 x_3} \int d^2 k_{1\perp} d^2 k_{2\perp} \times \frac{[\Gamma(x_i, \vec{k}_{i\perp})]^2}{(M_N^2 - M_0^2(x_1, \vec{k}_{1\perp}, x_2, \vec{k}_{2\perp}, x_3, \vec{k}_{3\perp}))^2}, \quad (21)$$

and for  $i \neq j$ :

$$I_{ij} = \frac{2}{(2\pi)^6} \int_0^{1-x_1} \frac{dx_2}{x_1 x_2 x_3} \int d^2 k_{1\perp} d^2 k_{2\perp} \times \frac{\Gamma(x_i, \vec{k}_{i\perp}) \Gamma(x_j, \vec{k}_{j\perp})}{(M_N^2 - M_0^2(x_1, \vec{k}_{1\perp}, x_2, \vec{k}_{2\perp}, x_3, \vec{k}_{3\perp}))^2}. \quad (22)$$

Due to the symmetries of the three-body wave function under exchange of particles 2 and 3, it follows that  $I_{22} = I_{33}$  and  $I_{12} = I_{13}$ .

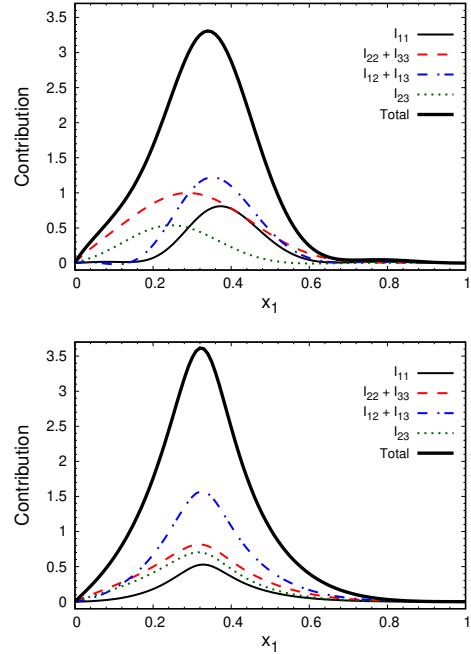


FIG. 5. Contributions to the PDF for the model I (lower panel) and II (upper panel)

The contributions to the PDF at vanishing  $Q^2$  are presented for the two considered models in the middle and upper panels of Fig. 4. The total PDF is also shown in each panel with a thick solid line. For both models a maximum of the PDF is seen at  $x \approx 1/3$ . As is seen the right panel, the model II with a positive



scattering length gives an almost flat behavior around  $x = 0.8$  for the PDF. Larger differences in the behavior of the contributions can also be observed for this set of parameters.

Interesting to observe that all the contributions have about the same size, and peaks around 0.35, despite we are measuring the PDF for the quark labeled by 1 with momentum fraction  $x_1$ . More variation of the peaks position are seen for  $a > 0$  where the vertex function has a node for model II (see Fig. 1), while the interplay with the denominator of the wave function where the smallest virtuality in the mass squared leads to fixed positions in all contributions around  $1/3$ . The contribution from  $I_{11}$  corresponding to a configuration, where quark 1 is picked up while the pair of quarks interacts, does not dominate, meaning that the symmetrization of the momentum component of the wave function is crucial for the nucleon PDF.

### B. Valence double parton distribution

Following Eq. (5), we write the valence contribution to the double quark distribution function as:

$$D_3(x_1, x_2; \vec{q}_\perp) = \frac{1}{(2\pi)^6} \int d^2 k_{1\perp} d^2 k_{2\perp} \times \Psi_3^\dagger(x_1, \vec{k}_{1\perp} + \vec{q}_\perp; x_2, \vec{k}_{2\perp} - \vec{q}_\perp; x_3, \vec{k}_{3\perp}) \times \Psi_3(x_1, \vec{k}_{1\perp}; x_2, \vec{k}_{2\perp}; x_3, \vec{k}_{3\perp}). \quad (23)$$

Our results for the DPDF calculated for  $\vec{q}_\perp = \vec{0}_\perp$  are shown for the two considered models in Fig. 6. For this particular value of transverse momentum  $D_3(x_1, x_2, \vec{0}_\perp)$  the double distribution is the probability density for finding quarks with momentum fraction  $x_1$  and  $x_2$ . In the upper panel it is seen that for model II, a strong suppression of the DPDF is seen for  $x_1 > 0.6$  as for the PDF. The model with  $a < 0$  gives a slightly more narrow DPDF. Observe the different shapes of the boundaries of the double quark distribution, giving complementary information with respect to the two-quark transverse momentum distribution, which is sensitive to the size of the nucleon, as we are going to discuss. The boundary for the higher probability density region for model I has an isosceles triangle shape, while for model II it has an isosceles trapezoid shape. The totally symmetric character of the wave function leads to the symmetry properties of the boundaries.

The triangular shaped boundary for model I, could be anticipated from the peak of largest probability for

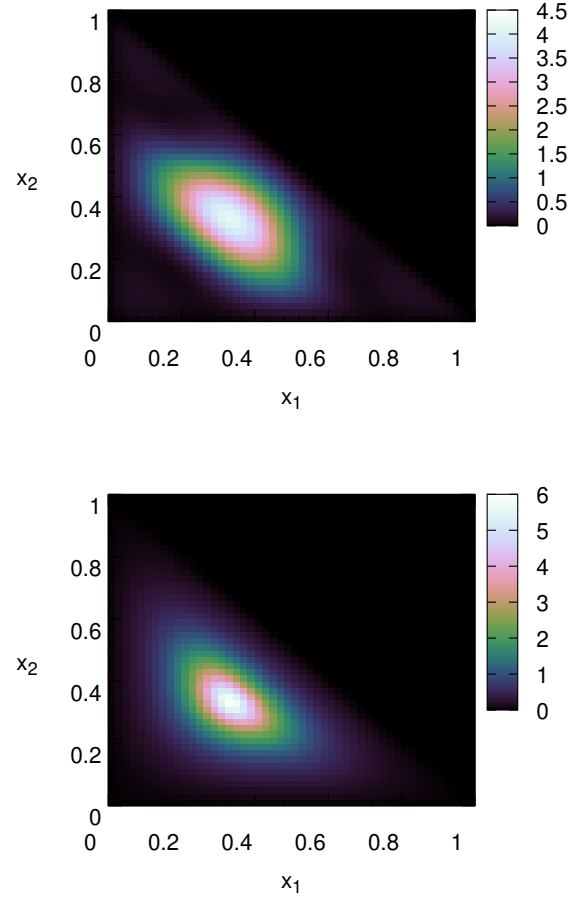


FIG. 6. Double quark distribution function,  $D_3(x_1, x_2, \vec{0}_\perp)$ , for the model I (lower panel) and II (upper panel).

$x_i \sim 0.3$ , being visible for 0.2 and above in Fig. 6, up to the boundary  $x_1 + x_2 = 1 - x_3$ . The trapezoid shaped boundary observed for model II can be associated with the strong damping of the PDF above  $x \sim 0.6$  seen in Fig. 5 and to its peak around  $x \sim 0.35$ , these two properties compete to provide the form seen in the upper panel of Fig. 6. Model II corresponds to an excited state and the nodes appearing in the vertex function for  $x$  around 0.2 and 0.6 provides such peculiar boundary form. What is noticeable is the sensitivity of the double PDF to the detail of the vertex function, while the valence transverse distributions are essentially sensitive to the size of the three quark configuration. Therefore, it is quite interesting to see that radially excited states have its particular imprints on the double quark distribution, as well as on the PDF.

### C. Transverse momentum distributions

The single quark transverse momentum distribution is associated with the probability density to find a quark with momentum  $k_{\perp}$ :

$$L_1(k_{1\perp}) = \frac{k_{1\perp}}{(2\pi)^6} \int_0^1 dx_1 \int_0^{1-x_1} dx_2 \int_0^{2\pi} d\theta_1 \times \int d^2 k_{2\perp} |\Psi_3(x_1, \vec{k}_{1\perp}, x_2, \vec{k}_{2\perp}, x_3, \vec{k}_{3\perp})|^2, \quad (24)$$

and the two-quark one reads

$$L_2(k_{1\perp}, k_{2\perp}) = \frac{k_{1\perp} k_{2\perp}}{(2\pi)^6} \int_0^1 dx_1 \int_0^{1-x_1} dx_2 \times \int_0^{2\pi} d\theta_1 \int_0^{2\pi} d\theta_2 |\Psi_3(x_1, \vec{k}_{1\perp}, x_2, \vec{k}_{2\perp}, x_3, \vec{k}_{3\perp})|^2. \quad (25)$$

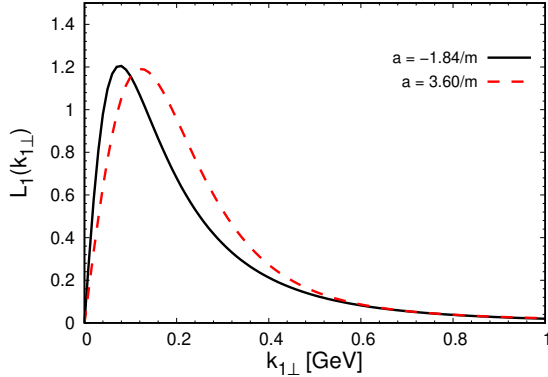


FIG. 7. One-quark transverse distribution vs  $k_{1\perp}$  for the model I ( $a = -1.84/m$ ) and II ( $a = 3.60/m$ ).

In Fig. 7 the single quark transverse momentum distribution from Eq. (24) is shown for models I and II. As expected, for model I with  $a = -1.84/m$ , the momentum distribution is narrower than for  $a = 3.6/m$ , as the radius for the former case is larger. The peak of the momentum distribution is about 0.08 GeV for model I and 0.12 GeV for model II, reflecting the larger size of the nucleon in model I compared to model II.

In Fig. 8 the two-quark transverse momentum distribution is shown for the model I (lower panel) and model II (upper panel). The more compact configuration of model II is reflected in the wider distribution, and the probability density peak is consistent with Fig. 7 to what was observed for the quark distribution.

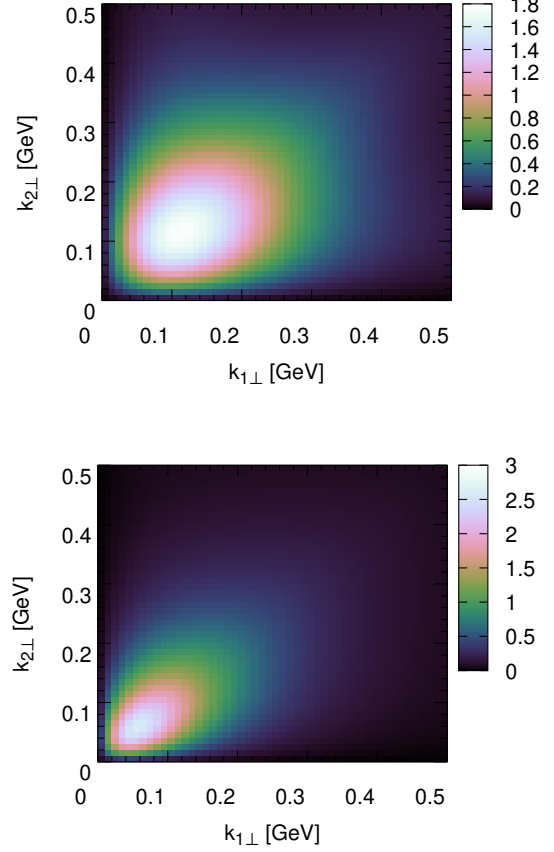


FIG. 8. Two-quark transverse distribution versus  $k_{1\perp}$  and  $k_{2\perp}$ , for the model I (lower panel) and II (upper panel).

## VI. SUMMARY

We study the Ioffe-time image, non-polarized longitudinal and transverse momentum distributions, and the double momentum distribution of the proton relying on a dynamical constituent quark light-front three-body model. The dynamics is based on the prevalence of the scalar diquark channel in the quark-quark interaction. We assume a minimal structure of quark-quark contact interaction, resembling the Nambu-Jona-Lasinio model, with the simplified assumption of factorization of the spin degree of freedom, and focusing on the totally symmetric momentum component of the light-front wave function. We study two possibilities, namely a diquark in a bound or a virtual state.

The three-body light-front Faddeev Bethe-Salpeter equations for the valence state was solved in the presence of virtual (model I) or bound (model II) diquark

states, for positive and negative scattering lengths, respectively. The contact interaction allows to simplify the integral equations for the Faddeev components of the vertex function, which depends only on the spectator quark longitudinal momentum fraction and transverse momentum. We have not used a momentum cut-off in the model as originally introduced in [26] and adopted the no-cutoff version [29]. This simplified dynamical model allowed to investigate only non-polarized quantities.

The adopted dynamical light-front model has two parameters: the constituent quark mass and scattering length. To determine these parameters the proton mass was fixed to its experimental value, and the binding energy as well as the scattering length were varied to have a qualitative fit of the Dirac form up to about 1 GeV<sup>2</sup>. It reproduces the Dirac form factor radius somewhat close to 1 fm, having the case of bound diquark a more compact configuration than the case with the virtual diquark state. These two possibilities produces quite different proton properties for the model with no cut-off. The bound diquark produces a deep three-quark non-physical state ( $M^2 < 0$ ), and the one associated with the proton is in this case an excited state, where the vertex function has nodes in the  $x$  dependence, while for the virtual diquark the nucleon is the ground state of the model. These two distinct natures of the valence state for model I and II allowed to study their observable consequences in the different momentum distributions and image.

Specifically, we computed several proton non-polarized quantities for the models (I) and (II):

- (i) the distribution amplitude (DA); it corresponds to the probability amplitude to find the quarks with given momentum fraction at the same transverse position. The model I has a narrow distribution on the  $(x_1, x_2)$  plane when compared to model II.
- (ii) the Ioffe-time image; it corresponds to the Fourier-transform of the DA in the Ioffe time, and gives the probability density of finding quarks along the light-like direction for quarks at the same transverse position. The quarks tend to have close Ioffe-time positions, and exhibit characteristic oscillations reflecting the size and mass of the system, besides the symmetry of the configuration space wave function.
- (iii) the quark distribution function; it corresponds to the probability density to find a quark with a given momentum fraction at the nucleon scale, peaked around  $x \sim 0.3$ , but distinguishing model I and II, the last one having nodes in the spectator function, and presenting a more localized distribution.
- (iv) the double quark distribution function; for  $\vec{q}_\perp = 0$ ; it corresponds to the probability density to find the quark with a given momentum fractions at the nucleon scale. The shape of the boundary with large probability to observe the momentum fractions distinguish model I and II, with an isosceles triangular and trapezoid shapes, for respectively, the ground-state and excited-state configurations.
- (v) the single quark transverse momentum distribution; is associated with the probability density to find a quark with a given transverse momentum and mainly sensitive to the size of the three-quark configuration and found peaked around 0.1 GeV.
- (vi) the double quark transverse momentum distribution; is associated with the probability density to find the quarks with a given transverse momentum and, again, mainly sensitive to the size of the three-quark configuration, a smaller region in momentum is found for the larger size of the proton for model I compared to the more compact configuration of the quarks in model II.

Future challenges for improving the nucleon effective model to be taken: the computation of the Bethe-Salpeter amplitude in the four-dimensional Minkowski space, which includes an infinite number of Fock-components, the introduction of a cut-off and the spin degree of freedom, which we expect will provide more insights into the nucleon structure.

## ACKNOWLEDGMENTS

This study was financed in part by Conselho Nacional de Desenvolvimento Científico e Tecnológico (CNPq) under the grant 308486/2015-3 (TF). E.Y. thanks for the financial support of the grants #2016/25143-7 and #2018/21758-2 from FAPESP. We thank the FAPESP Thematic Projects grants #13/26258-4 and #17/05660-0.

- 
- [1] S. J. Brodsky, H.-C. Pauli, and S. S. Pinsky, Quantum chromodynamics and other field theories on the light cone, *Phys. Rep.* **301**, 299 (1998), arXiv:hep-ph/9705477 [hep-ph].
  - [2] B. Bakker, A. Bassetto, S. Brodsky, W. Broniowski, S. Dalley, T. Frederico, S. Glazek, J. Hiller, C.-R. Ji, V. Karmanov, *et al.*, Light-Front Quantum Chromodynamics: A framework for the analysis of hadron physics, *Nucl. Phys. B Proc. Suppl.* **251**, 165 (2014).
  - [3] J. Arrington, C. A. Gayoso, P. C. Barry, V. Berdnikov, D. Binosi, L. Chang, M. Diefenthaler, M. Ding, R. Ent, T. Frederico, and *et al.*, Revealing the structure of light pseudoscalar mesons at the electron-ion collider, *J. Phys. G: Nucl. Part. Phys.* **48**, 075106 (2021).
  - [4] S. W. Li, P. Lowdon, O. Oliveira, and P. J. Silva, The generalised infrared structure of the gluon propagator, *Phys. Lett. B* **803**, 135329 (2020).
  - [5] X.-D. Ji, J.-P. Ma, and F. Yuan, Generalized counting rule for hard exclusive processes, *Phys. Rev. Lett.* **90**, 241601 (2003), arXiv:hep-ph/0301141.
  - [6] W. de Paula, E. Ydrefors, J. H. Alvarenga Nogueira, T. Frederico, and G. Salmè, Observing the Minkowskian dynamics of the pion on the null-plane, *Phys. Rev. D* **103**, 014002 (2021), arXiv:2012.04973 [hep-ph].
  - [7] V. Gribov, B. Ioffe, and I. Pomeranchuk, What is the range of interactions at high-energies, *Sov. J. Nucl. Phys.* **2**, 549 (1966).
  - [8] B. Ioffe, Space-time picture of photon and neutrino scattering and electroproduction cross-section asymptotics, *Phys. Lett. B* **30**, 123 (1969).
  - [9] V. Braun, P. Gornicki, and L. Mankiewicz, Ioffe - time distributions instead of parton momentum distributions in description of deep inelastic scattering, *Phys. Rev. D* **51**, 6036 (1995), arXiv:hep-ph/9410318.
  - [10] G. A. Miller and S. J. Brodsky, The Frame-Independent Spatial Coordinate  $\hat{z}$ : Implications for Light-Front Wave Functions, Deep Inelastic Scattering, Light-Front Holography, and Lattice QCD Calculations, *Phys. Rev. C* **102**, 022201 (2020), arXiv:1912.08911 [hep-ph].
  - [11] B. Joó, J. Karpie, K. Orginos, A. V. Radyushkin, D. G. Richards, R. S. Sufian, and S. Zafeiropoulos, Pion valence structure from Ioffe-time parton pseudodistribution functions, *Phys. Rev. D* **100**, 114512 (2019), arXiv:1909.08517 [hep-lat].
  - [12] R. Abdul Khalek and *et al.*, Science Requirements and Detector Concepts for the Electron-Ion Collider: EIC Yellow Report (2021), arXiv:2103.05419 [physics.ins-det].
  - [13] M. Diehl, Generalized parton distributions, *Phys. Rep.* **388**, 41 (2003), arXiv:hep-ph/0307382 [hep-ph].
  - [14] S. Meißner, K. Goeke, A. Metz, and M. Schlegel, Generalized parton correlation functions for a spin-0 hadron, *JHEP* **2008** (08), 038–038.
  - [15] S. Meissner, A. Metz, and M. Schlegel, Generalized parton correlation functions for a spin-1/2 hadron, *JHEP* **08**, 056, arXiv:0906.5323 [hep-ph].
  - [16] C. Lorcé, B. Pasquini, and M. Vanderhaeghen, Unified framework for generalized and transverse-momentum dependent parton distributions within a 3Q light-cone picture of the nucleon, *JHEP* **2011** (5), 041.
  - [17] C. Lorcé and B. Pasquini, Structure analysis of the generalized correlator of quark and gluon for a spin-1/2 target, *JHEP* **2013** (9), 138.
  - [18] D. Treleani and G. Calucci, Inclusive and Exclusive Cross-Sections, Sum Rules, *Adv. Ser. Direct. High Energy Phys.* **29**, 29 (2018), arXiv:1707.00271 [hep-ph].
  - [19] P. Bartalini and J. R. Gaunt, eds., *Multiple Parton Interactions at the LHC*, Vol. 29 (WSP, 2019).
  - [20] B. Blok, Y. Dokshitzer, L. Frankfurt, and M. Strikman, Four-jet production at LHC and Tevatron in QCD, *Phys. Rev. D* **83**, 071501(R) (2011).
  - [21] Bali, Gunnar S. and Diehl, Markus and Gläfle, Benjamin and Schäfer, Andreas and Zimmermann, Christian, Double parton distributions in the nucleon from lattice QCD, arXiv:2106.03451 [hep-lat] (2021).
  - [22] M. Traini, M. Rinaldi, S. Scopetta, and V. Vento, The effective cross section for double parton scattering within a holographic AdS/QCD approach, *Phys. Lett. B* **768**, 270 (2017), arXiv:1609.07242 [hep-ph].
  - [23] M. Rinaldi and F. A. Ceccopieri, Double parton scattering and the proton transverse structure at the LHC, *JHEP* **2019** (9), 097.
  - [24] J. Vary, H. Honkanen, J. Li, P. Maris, S. Brodsky, A. Harindranath, G. de Teramond, P. Sternberg, E. Ng, and C. Yang, Hamiltonian light-front field theory in a basis function approach, *Phys. Rev. C* **81**, 035205 (2010), arXiv:0905.1411 [nucl-th].
  - [25] C. Mondal, S. Xu, J. Lan, X. Zhao, Y. Li, D. Chakrabarti, and J. P. Vary (BLFQ Collaboration), Proton structure from a light-front Hamiltonian, *Phys. Rev. D* **102**, 016008 (2020).
  - [26] T. Frederico, Null-plane model of three bosons with zero-range interaction, *Phys. Lett. B* **282**, 409 (1992).
  - [27] W. R. B. de Araújo, J. P. B. C. de Melo, and T. Frederico, Faddeev null-plane model of the nucleon, *Phys. Rev. C* **52**, 2733 (1995).
  - [28] E. F. Suisso, J. P. B. C. de Melo, and T. Frederico, Relativistic dynamics of Qqq systems, *Phys. Rev. D* **65**, 094009 (2002).
  - [29] J. Carbonell and V. A. Karmanov, Three-boson relativistic bound states with zero-range two-body interaction, *Phys. Rev. C* **67**, 037001 (2003).

- [30] E. Ydrefors, J. H. Alvarenga Nogueira, V. Gigante, T. Frederico, and V. A. Karmanov, Three-body bound states with zero-range interaction in the Bethe–Salpeter approach, *Phys. Lett. B* **770**, 131 (2017), arXiv:1703.07981 [nucl-th].
- [31] E. Ydrefors, J. H. Alvarenga Nogueira, V. A. Karmanov, and T. Frederico, Solving the three-body bound-state Bethe-Salpeter equation in Minkowski space, *Phys. Lett. B* **791**, 276 (2019), arXiv:1903.01741 [hep-ph].
- [32] E. Ydrefors, J. H. Alvarenga Nogueira, V. A. Karmanov, and T. Frederico, Three-boson bound states in Minkowski space with contact interactions, *Phys. Rev. D* **101**, 096018 (2020), arXiv:2005.07943 [hep-ph].
- [33] O. Hen, G. A. Miller, E. Piasetzky, and L. B. Weinstein, Nucleon-nucleon correlations, short-lived excitations, and the quarks within, *Rev. Mod. Phys.* **89**, 045002 (2017).
- [34] G. Eichmann, H. Sanchis-Alepuz, R. Williams, R. Alkofer, and C. S. Fischer, Baryons as relativistic three-quark bound states, *Prog. Part. Nucl. Phys.* **91**, 1 (2016), arXiv:1606.09602 [hep-ph].
- [35] M. Y. Barabanov, M. A. Bedolla, W. K. Brooks, G. D. Cates, C. Chen, Y. Chen, E. Cisbani, M. Ding, G. Eichmann, R. Ent, J. Ferretti, R. W. Gothe, T. Horn, S. Liuti, C. Mezrag, A. Pilloni, A. J. R. Puckett, C. D. Roberts, P. Rossi, G. Salmé, E. Santopinto, J. Segovia, S. N. Syritsyn, M. Takizawa, E. Tomasi-Gustafsson, P. Wein, and B. B. Wojtsekhowski, Diquark correlations in hadron physics: Origin, impact and evidence, *Prog. Part. Nucl. Phys.* **116**, 103835 (2021), arXiv:2008.07630 [hep-ph].
- [36] S. P. Klevansky, The Nambu-Jona-Lasinio model of quantum chromodynamics, *Rev. Mod. Phys.* **64**, 649 (1992).
- [37] A. Francis, P. de Forcrand, R. Lewis, and K. Maltman, Diquark properties from full QCD lattice simulations, arXiv:2106.09080 [hep-lat] (2021).
- [38] K. Fukushima, J. M. Pawłowski, and N. Strodthoff, Emergent Hadrons and Diquarks, arXiv:2103.01129 [hep-ph] (2021).
- [39] J. Ferretti, Effective Degrees of Freedom in Baryon and Meson Spectroscopy, *Few-Body Syst.* **60**, 17 (2019).
- [40] W. Xiong *et al.*, A small proton charge radius from an electron–proton scattering experiment, *Nature* **575**, 147 (2019).
- [41] O. Oliveira, P. J. Silva, J.-I. Skullerud, and A. Sternbeck, Quark propagator with two flavors of O(a)-improved Wilson fermions, *Phys. Rev. D* **99**, 094506 (2019), arXiv:1809.02541 [hep-lat].
- [42] L. H. Thomas, The Interaction Between a Neutron and a Proton and the Structure of  $H^3$ , *Phys. Rev.* **47**, 903 (1935).
- [43] Z. Ye, J. Arrington, R. J. Hill, and G. Lee, Proton and Neutron Electromagnetic Form Factors and Uncertainties, *Phys. Lett. B* **777**, 8 (2018), arXiv:1707.09063 [nucl-ex].